Report

Regulation of Frizzled-Dependent Planar Polarity Signaling by a V-ATPase Subunit

Tobias Hermle,[1,2] Deniz Saltukoglu,[1,3] Julian Grünewald,[1,2] Gerd Walz,[2] and Matias Simons[1,2,4,*]
[1]Center for Systems Biology (ZBSA), University of Freiburg, Habsburgerstrasse 49, 79104 Freiburg, Germany
[2]Renal Division, Department of Medicine, University Hospital Freiburg, Hugstetter Straße 55, 79106 Freiburg, Germany
[3]Spemann Graduate School of Biology and Medicine, University of Freiburg, Albertstrasse 19A, 79104 Freiburg, Germany
[4]Freiburg Initiative for Systems Biology (FRISYS), Schänzlestrasse 1, 79104 Freiburg, Germany

Summary

Frizzled (Fz) is a seven-pass transmembrane receptor that acts in both Wingless (Wg) and planar cell polarity (PCP) pathways. A prerequisite for PCP signaling is the asymmetric subcellular distribution of Fz [1–3]. However, the regulation of Fz asymmetry is currently not well understood. Here we describe that the transmembrane protein CG8444 (here termed VhaPRR) is needed for PCP signaling in *Drosophila*. VhaPRR is an accessory subunit of the vacuolar (V)-ATPase proton pump [4], but it also functions as a receptor for (pro)renin (PRR) in mammals [5, 6]. We show that VhaPRR function is tightly linked with Fz but not other PCP core proteins. Fz fails to localize asymmetrically in the absence of VhaPRR, and this is accompanied by prehair mispolarization of pupal wing cells. In addition, VhaPRR forms a protein complex with Fz receptors and interacts genetically with Fz in the *Drosophila* eye. VhaPRR also acts as a modulator of canonical Wnt signaling in larval and adult wing tissue. Its loss leads to an expansion of the Wg morphogen gradient and a reduction of Wg target gene expression. The requirement for additional V-ATPase subunits suggests that proton fluxes contribute to normal Fz receptor function and signaling.

Results

The planar cell polarity (PCP) pathway polarizes cells in the plane of a tissue in a cell-autonomous and nonautonomous manner. The pathway is best understood in *Drosophila*, where it regulates a number of morphogenetic processes, such as the precise ommatidial arrangement in the eye and the orientation of hairs and bristles of the wing and notum. Because it shares molecular components such as Frizzled (Fz) with the canonical Wnt pathway, it is also named the noncanonical Wnt pathway. Both pathways are essential for numerous developmental processes and are deregulated in many human diseases [1, 2]. We previously reported the involvement of the sodium-proton exchanger, Nhe2, in Fz-mediated planar polarity signaling in *Drosophila* [7]. Subsequently, a genome-wide RNA interference (RNAi) screen for notum bristle phenotypes suggested that the knockdown of *CG8444* causes bristle

*Correspondence: matias.simons@uniklinik-freiburg.de

polarity defects [8]. Although *CG8444* has not been functionally characterized in *Drosophila*, it has been termed *VhaM8-9* because of its sequence homology with an accessory subunit of the vacuolar proton pump, V-ATPase [4]. Like Nhe2, the V-ATPase extrudes protons from the cytosol into organelles and/or the extracellular space. The mammalian ortholog functions as a receptor for renin and prorenin (PRR), and hypomorphic PRR mutations cause mental retardation and epilepsy in humans [9]. Our name VhaPRR reflects the proposed dual function of the protein and the homology with PRR (as compared with *VhaPPA1*, another V-ATPase subunit).

VhaPRR Is Required for Planar Cell Polarity

Confirming the finding of the bristle screen, the expression of *VhaPRR* RNAi (RNAi-1) with another notum driver, *apterous (ap)-GAL4*, caused severe planar polarity defects in the anterior-posterior orientation of sensory bristles or microchaetae (Figures 1B and 1E). However, we also detected abnormalities in notum bristle morphology and number, suggesting defects in other processes. In the wing, the knockdown of *VhaPRR* with several drivers caused PCP defects in combination with growth and vein defects. The PCP defects were strongest in the proximal *dpp* or *patched* (*ptc*) expression domain between veins L3 and L4. Here *VhaPRR* knockdown caused multiple wing hair and hair mispolarization phenotypes (Figure 1G; Figures 2A, 2B, and 2D; see also Figure S4B' available online). As visualized by GFP coexpression in the pupal stage, defects in prehair polarity were confined to the *dpp* and *ptc* expression domain, suggesting cell-autonomous PCP defects (Figure S4B'; data not shown). In addition to the loss-of-function analysis, we overexpressed *VhaPRR* in the wing. The overexpression in the *dpp* stripe caused swirls and multiple wing hairs in the proximal part of the wing (Figure 1H). Interestingly, *engrailed* (*en*)-*GAL4*-mediated *VhaPRR* overexpression also led to hairs pointing toward the wild-type anterior domain that also can be seen when Fz is overexpressed (Figures 1I and 1J) [10, 11]. However, similar to the knockdown, the mispolarization seemed to be confined to the expression domain.

To exclude off-target effects that may be associated with RNAi knockdown, we used an additional RNAi line (termed RNAi-2). The RNAi sequences are nonoverlapping, and their expression generally caused comparable phenotypes. Experiments were performed with both RNAi lines, as indicated in the figures. We also detected a partial rescue of the wing phenotype caused by *nubbin-GAL4*-mediated *VhaPRR* knockdown when coexpressing the human ortholog PRR-EGFP (26% identity with *VhaPRR/dPRR*), but not with an N-terminal truncation of PRR lacking parts of the extracellular domain (Figures S2A–2C; data not shown). Moreover, overexpressed *VhaPRR* can be efficiently knocked down with *VhaPRR* RNAi (Figures S2G and S2H).

VhaPRR Regulates Fz Trafficking in the Pupal Wing

We next analyzed different pupal stages between 28 and 36 hr after pupal formation (APF). During this period in pupal development, active PCP signaling leads to asymmetric PCP protein localization on the apical circumference of the hexagonally shaped pupal wing cells and subsequent polarized prehair
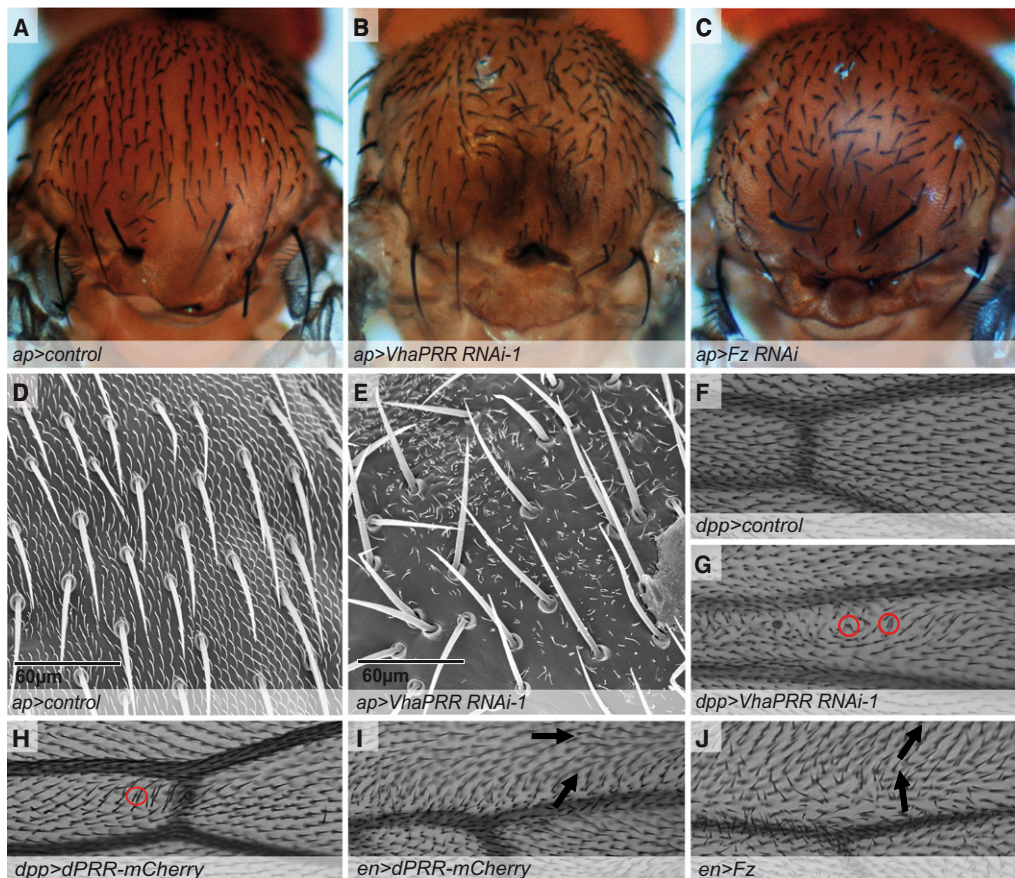
Figure 1. VhaPRR Is Required for Planar Cell Polarity

(A–C) *VhaPRR* RNAi-1 expression in the notum under the control of *ap-GAL4* results in planar cell polarity (PCP) defects (B). Anterior-posterior alignment of sensory bristles is impaired, particularly in the medial compartment. In addition, the number and spacing of bristles is altered. Control RNA interference (RNAi) (A) and Frizzled (Fz) RNAi (C) are shown for comparison. Note that the scutellum is deformed when *ap-GAL4* is expressed at 29°C.

(D and E) Scanning electron micrographs show the notum in higher resolution. In addition to the sensory bristles, the small epidermal hairs are mispolarized and not restricted to one hair per cell in *VhaPRR*-silenced nota (E).

(F–H) The *dpp* and *ptc* expression domain runs as a narrow stripe between the longitudinal veins L3 and L4 (see Figure S4 for the marking of the knockdown area in pupal wings). Images show details of the proximal anterior crossvein area (left) of the expression domain. Anterior is up.

(F) Wing hairs point in the proximodistal direction and show correct alignment in *dpp-GAL4*/+ wings.

(G) Wings expressing *VhaPRR* RNAi-1 with *dpp-GAL4* show cell-autonomous PCP defects, including wing hair misorientation and multiple wing hairs (red circle), in the proximal part. In addition to the PCP phenotypes, the *dpp* compartment is reduced in size, and vein material is either lost or ectopic.

(H–J) The overexpression of *VhaPRR* (the transgene is termed dPRR-mCherry) [40] also causes PCP defects. Note that when *VhaPRR* is expressed with *en-GAL4* (I), the hairs point from the posterior (bottom arrow) to the wild-type anterior compartment (top arrow). Unlike *en>Fz*, which shows nonautonomous effects (J), the defects are confined to the posterior domain (I).

formation (Figures 2A, 2C, and 2E; Figure S5). Fz is transported in vesicles to distal cell junctions on proximodistally oriented microtubules, leading to a peak in Fz asymmetry at ~30 hr APF and prehair formation on the distal part of the apical surface at ~32 hr APF [12]. We observed that in *ptc>VhaPRR* RNAi wings, Fz was strikingly mislocalized at 28 hr APF. Fz did not localize to distal cell junctions (marked by E-cadherin) and was found in puncta away from the junctions (Figures 2A, 2B, and 2D; Figure S4A). Fz puncta were not positive for another PCP core protein, Flamingo (Fmi), suggesting a specific defect in Fz trafficking (Figure S4A; data not shown). At 32 and 36 hr APF, Fz localization was more junctional but also less asymmetric compared with the typical zigzag localization pattern of Fz outside of the *ptc* domain (Figures 2A–2E; Figure S4). This correlated with a delay in prehair formation and with defects in prehair polarity (Figures 2B–2E; Figures S4B and S4C). The severity and dimension of the Fz localization

defect was generally more pronounced at earlier stages, when it affected the entire *ptc* domain (Figure 2A; data not shown). At later stages, this defect and also the hair polarity defects were confined to the area surrounding the anterior crossvein, suggesting compensatory mechanisms, particularly in the more distal areas (Figure S4C). We also found that *VhaPRR* knockdown led to larger and irregular cell shapes. This phenotype was visible at all time points examined, even before 28 hr APF (Figures 2A–2E; Figure S4A'; data not shown). It has previously been reported that hexagonal cell packing in the pupal wing is controlled by PCP factors, including Fz, but may also be affected by cell ablation [13, 14]. Because we observed an increased number of cleaved Caspase 3 positive cells in the *ptc* domain after *VhaPRR* knockdown, the cell shape changes could indeed occur as a consequence of apoptotic cell ablation (Figure S5A). Interestingly, the overexpression of the proapoptotic *Eiger* (under control of the
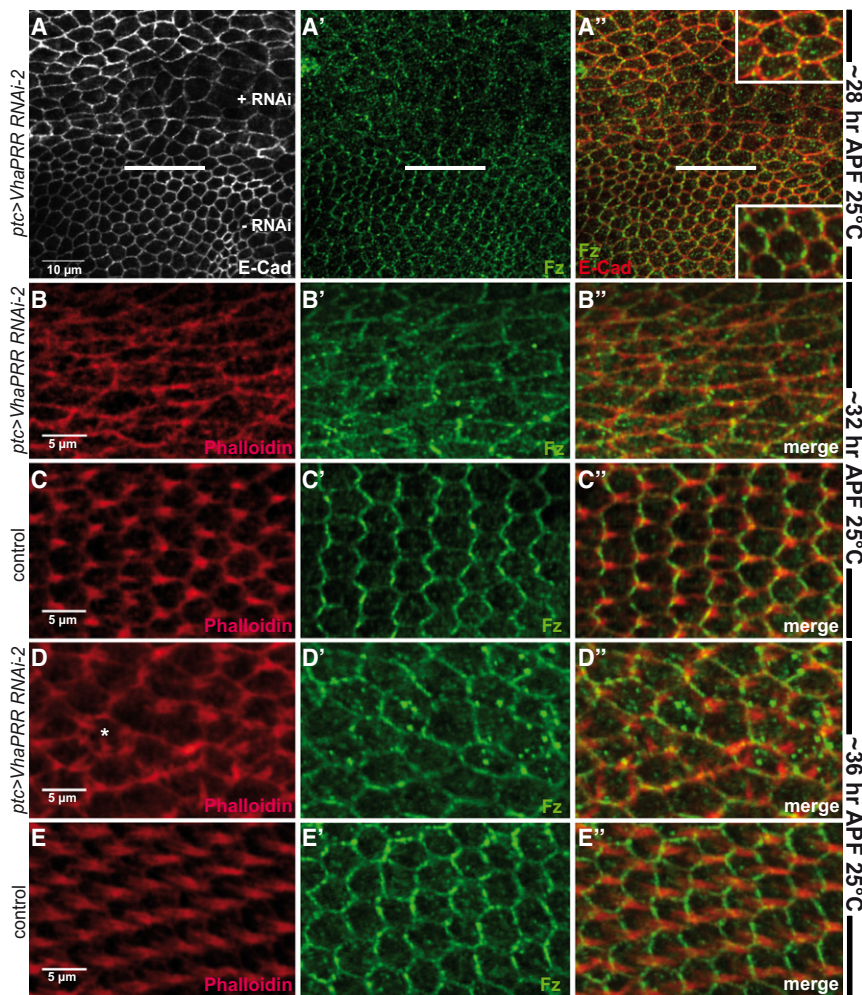
Figure 2. VhaPRR Is Required for Correct Fz Localization in the Pupal Wing

(A–E) *VhaPRR* RNAi was expressed using *ptc-GAL4*, and pupal wings were examined at ~28 hr (A), 32 hr (B and C), and 36 hr (D and E) after pupal formation (APF) at 25°C. In (A), an overview of the pupal wing with *ptc* and wild-type domains is shown. The *ptc* domain comprises the area above vein L4 (L4 position is indicated by the white bar; see also Figure S4). Distal is to the right and posterior is down. An enlargement of an area inside the *ptc* domain is shown in (B) and (D), and an area posterior to the *ptc* domain is shown in (C) and (E).

(A–A″) At ~28 hr APF, the cell shape marked with E-cadherin (E-Cad; A and A″) is larger and irregular compared with the hexagonal cell morphology in the posterior half without *VhaPRR* RNAi expression. In addition, Fz localizes away from distal cell junctions in cytosolic puncta in the *ptc* domain (A'). A merge shows membrane localization of Fz in wild-type cells, but not in *VhaPRR*-silenced cells (A″). The higher magnification insets show Fz accumulation at distal cell junctions marked by E-cadherin in wild-type cells and cytosolic Fz puncta in knockdown cells.

(B–C″) At ~32 hr APF, prehairs start to form outside (B), but not inside (C), the *ptc* domain, suggesting a delay in prehair formation. Fz localization is still less asymmetric and more cytosolic in the *ptc* domain compared with the typical zigzag pattern in the wild-type tissue (B' and C'; for Fz and Fmi at 34 hr APF, see Figure S4A).

(D–E″) At ~36 hr APF, prehairs are significantly longer. Mispolarization of prehairs and multiple wing hair cells (*) can be seen in the *ptc* domain (D), whereas in the control area, hairs are straight (E). (D') Fz assumes a more cortical localization at ~36 hr APF, especially in more distal regions of the ptc domain (Figure S4C; for 34 hr APF, the visualization of the *ptc* expression domain, and a wild-type *ptc* domain, see also Figure S4).

temperature-dependent *GAL80ts*) phenocopied the cell shape changes but not the defects in Fz localization and prehair polarity (Figures S5B and S5C). Therefore, we suggest that VhaPRR has multiple effects on pupal wing morphogenesis. Increased apoptosis and/or Fz-dependent cell packing defects may account for the alterations in cell morphology, and a specific effect on Fz trafficking during critical stages in pupal development leads to PCP defects.

VhaPRR Interacts Genetically and Physically with Fz in the PCP Pathway

To study the relationship between VhaPRR and Fz in more detail, we turned to the *Drosophila* eye, a tissue very suitable for quantitative PCP analysis and genetic interaction experiments. In the eye, planar polarity regulates the orientation and chiral organization of entire ommatidia, as well as the specification of individual photoreceptors (such as R3 and R4) within the ommatidium [15]. The *sevenless* (*sev*) enhancer-driven expression is useful for PCP analysis, because it is transiently expressed in both cells of the R3/R4 pair at a time when PCP signaling is particularly active. Because Fz is required for R3 specification, *sev-GAL4*-mediated Fz overexpression leads to a high number of symmetrical ommatidia that contain two R3 cells instead of the normal R3/R4 pair on the polar side of the ommatidia (Figures 3A–3E) [16, 17]. Total PCP defects of *sev-Fz* but not *sev-Dishevelled (Dsh)* or *sev-Fmi* eyes were

suppressed by one copy of the *P* element (EY03616) positioned in the 5′ untranslated region of the *VhaPRR* gene. This insertion causes early lethality when it is heterozygous over deficiency ED9204, which uncovers the *VhaPRR* locus. It may therefore be assumed that the insertion results in a mutant allele of *VhaPRR* (*VhaPRR¹*). The *sev-Fz* phenotype was not suppressed by a revertant chromosome devoid of the *P* element (Figures 3A, 3B, and 3E) but was enhanced by the cooverexpression of *VhaPRR* (Figure 3B). The suppression of the Fz phenotype could also be achieved by coexpressing *VhaPRR* RNAi and was even more pronounced when counting only symmetrical ommatidia instead of total PCP defects (Figures 3A and 3C). The expression of the RNAi alone very rarely caused PCP defects. However, these defects were enhanced by one copy of *VhaPRR¹*, providing further support for the specificity of the RNAi (Figure S1B). Together, these results suggest that VhaPRR interacts genetically with Fz, but not with other PCP core proteins.

We next tested for physical interaction with Fz receptors. Because of the evolutionary conservation of *VhaPRR* and the positive rescue experiment (Figures S2 and S3), we used V5-tagged XPRR to test for coimmunoprecipitation with FLAG-tagged XFz8 (X for *Xenopus*). Unlike control transmembrane proteins, PRR and Fz8 coimmunoprecipitated each other reciprocally in HEK293T cells (Figure 3F; data not shown), confirming most recent results by others [18]. PRR
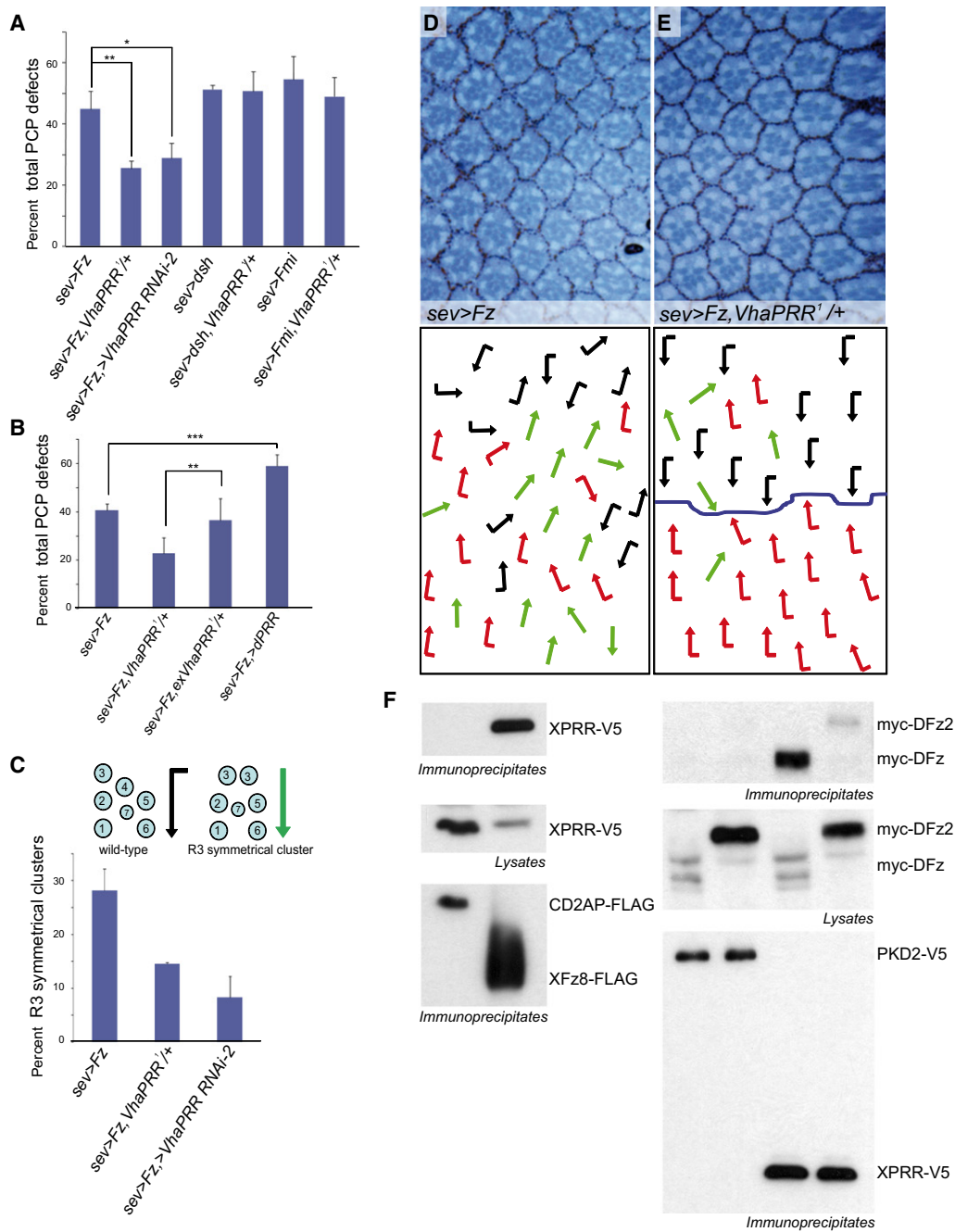
Figure 3. VhaPRR Interacts Genetically and Physically with Fz

(A–C) The *sev-Fz* phenotype is suppressed by *VhaPRR[1]* or by coexpression of *VhaPRR* RNAi.

(D and E) Tangential eye sections of adult eyes (top) with respective schematic representations (bottom). Dorsal and ventral ommatidia are depicted with black and red arrows, respectively. Sections are around the equator, which is not visible in (D) because of the strong *sev-Fz* phenotype consisting of symmetrical clusters (green arrows; schematic diagram in B), rotation defects, and chirality inversions.

(E) Heterozygous *VhaPRR[1]* reduces PCP defects in the *sev-Fz* phenotype, particularly the number of symmetrical clusters, and also restores the equator (blue line). Quantification for total PCP defects is shown in (A) and (B), and quantification of only symmetrical clusters is shown in (C). There is no genetic interaction with other PCP core genes such as Dsh and Fmi (data are mean ± standard deviation [SD] of at least three eyes with over 300 ommatidia scored, two-tailed unpaired t test, **p < 0.001 and *p < 0.05).

(B) A revertant chromosome with excision of *P* element EY03616 (*exVhaPRR[1]*) does not suppress sev-Fz phenotypes compared with the chromosome containing the *P* element (*VhaPRR[1]*). The cooverexpression of *dPRR* enhances *sev-Fz* PCP defects (data are mean ± SD of at least four eyes with over 450 ommatidia scored, two-tailed unpaired t test, ***p < 0.0001 and **p < 0.005).

(F) V5-tagged XPRR (XPRR-V5) was coexpressed with FLAG-tagged XFz8 and a control protein (CD2AP-FLAG) in HEK293T cells (X for *Xenopus*). After immunoprecipitation with anti-FLAG, XPRR-V5 was present in immunoprecipitates formed by XFz8-FLAG, but not by CD2AP-FLAG (left). In a similar fashion, DFz bound to XPRR-V5, but not to the control transmembrane protein PKD2-V5 immunoprecipitates (D for *Drosophila*; DFz corresponds to Fz). DFz2 also bound to XPRR-V5, albeit with a lower affinity (right). Each protein band is labeled with the corresponding protein name on the right side of the blot.
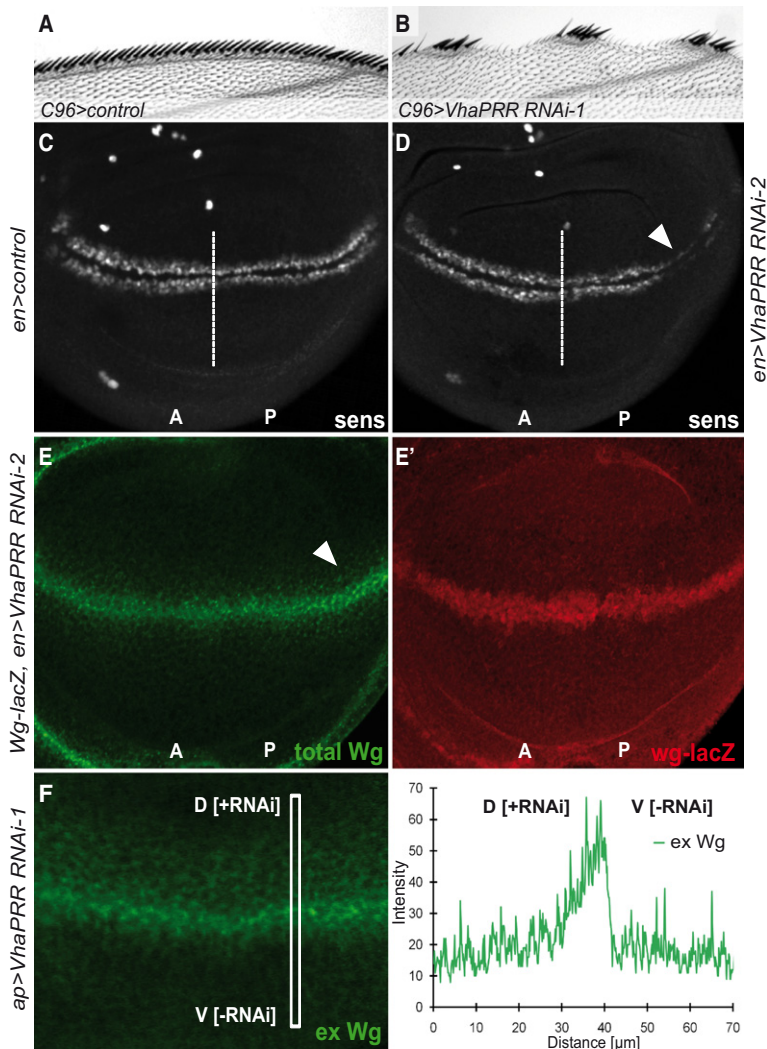
Figure 4. VhaPRR Modulates Canonical Wg Signaling

(A) Anterior wing margin of *C96-GAL4/+* showing sensory bristles. Formation of sensory bristles is controlled by peak levels of canonical Wnt signaling and the expression of target genes like *senseless* (sens) along the dorsoventral boundary.

(B) Silencing of *VhaPRR* in the area around the dorsoventral boundary using *C96-GAL4* results in intermittent loss of sensory bristles, indicating a loss-of-function Wg phenotype.

(C and D) Confocal images of wing discs from third instar larvae expressing GAL4 alone (C) or *VhaPRR* RNAi (D) in the posterior (P) compartment with *en-GAL4*. Dorsal is up. The anterior-posterior border is indicated by a white bar, as judged by immunostaining of engrailed (not shown). Compared with *en-GAL4/+*, sens staining is slightly reduced in the P compartment of *en>VhaPRR* RNAi-2 discs, particularly in more lateral regions (arrowhead).

(E) Wing discs stained by anti-Wg antibody displaying an increase of total Wg protein in lateral regions of the P compartment (arrowhead).

(E') Staining of a *wg-lacZ* reporter with anti-β-gal antibody, however, does not show an expansion.

(F) A protocol that exclusively stains extracellular Wingless reveals an extracellular Wg fraction that is diffusely increased in the dorsal (D) compartment when *VhaPRR* RNAi-1 is expressed with *ap-GAL4*. The area in the white box was used for quantification (graph). All images are projections of several wing disc sections (see also Figure S6 for more images, Dll staining, and Wg/sens staining with *ap-GAL4*).

also bound with high affinity to myc-DFz and with low affinity to myc-DFz2 (D for *Drosophila*; Figure 3F). Whereas DFz2 only functions in canonical Wingless (Wg), DFz functions in both canonical Wg and PCP signaling [19]. Taken together, the combined genetic and biochemical analysis argues for a common role of Fz receptors and VhaPRR in PCP signaling, possibly carried out in close proximity in the plasma membrane and/or transport vesicles.

VhaPRR Modulates the Wg Morphogen Gradient and the Expression of Wg Target Genes

Because Fz also functions in the canonical Wnt or Wg pathway, we wondered whether VhaPRR is involved in this pathway as well. During wing development, Wg controls the differentiation of sensory margin bristle neurons at the dorsoventral (DV) boundary via the β-catenin-dependent pathway through activation of target genes such as *senseless* (sens). Expressing *VhaPRR* RNAi throughout the DV boundary with *C96-GAL4* resulted in areas without bristles in the adult wing margin (Figures 4A and 4B). Immunostaining of the wing discs revealed that sens was slightly reduced and irregular compared to the control experiment, possibly explaining the defects in the adult tissue. Apoptotic rates were not increased in the wing disc (data not shown). The same effect on *sens* expression was seen with two other wing drivers, *en-GAL4*

and *ap-GAL4*, in their respective expression domains (Figures 4C and 4D; Figures S6C–S6E). By contrast, *Distalless* (Dll) expression was not significantly altered, suggesting that high-threshold Wg signaling is predominantly affected (Figure S6E'; data not shown). *Wg* is expressed and secreted at the dorsoventral boundary, resulting in a gradient of extracellular Wg with decreasing levels of Wg on either side of the boundary. We found that silencing *VhaPRR* enhanced the Wg gradient (Figure 4E; Figure S6C). Confinement of *wg* gene expression at the dorsoventral boundary is the result of Notch signaling and of its own self-repression [20, 21]. However, using a *wg-lacZ* reporter line, we detected no difference in the spatial pattern of *wg*-expressing cells (Figure 4E'). This suggests that the increase in Wg protein is not due to an increased Wg production. Next, we stained for extracellular Wg protein and found a similar expansion as for total Wg in the absence of VhaPRR (Figure 4F; Figure S6D). Similar findings have been reported upon overexpression of the glypican *dally-like* (dlp), which promotes the spread of Wg on the basal surface of the wing disc epithelium [22, 23]. Based on our immunostainings, dlp expression was not altered in the absence of VhaPRR (data not shown). Similarly, the canonical Fz2 receptor and its coreceptor arrow, which can also bind and internalize Wg, did not show an altered localization pattern, at least not with the available antibodies (data not shown) [24, 25]. Taken together, our results demonstrate that VhaPRR modulates the Wg morphogen gradient and the expression of a high-level Wg target gene. The mechanism may not include altered steady-state localization of dlp and Fz2, but it is possible that the activity of these components is altered by *VhaPRR* deficiency. For example, the signaling and internalization activity of the Fz receptor complex may be reduced, and/or the Wg spreading activity of glypicans may be enhanced [22].

The Role of Other V-ATPase Subunits in PCP and Wg Signaling

In mammals, it has been proposed that VhaPRR may act both as a receptor for (pro)renin in the renal control of blood pressure and as a subunit of the V-ATPase [6]. Very recent data from *Xenopus laevis* suggests that the renin-binding function of PRR is not involved in Wnt signaling. Furthermore, it was shown that V-ATPase inhibitors block Wnt signaling by preventing LRP6 phosphorylation in intracellular vesicles [18]. Because there are no clear renin homologs in the fly, we turned our attention to the V-ATPase. V-ATPases are evolutionarily conserved ATP-driven proton pumps composed of two multicomponent subcomplexes, the membrane-bound V_o, which mediates electrogenic proton translocation, and the peripheral V_1, which is responsible for ATP hydrolysis. Many of the 15 *Drosophila* subunits are expressed by different paralogs and splice variants. It is believed that this complexity contributes to the functional diversity of the V-ATPase in different organelles, cells, and tissues [4]. Biochemically, VhaPRR has been found to associate with the membraneous V_o part of the V-ATPase, but it is unknown whether it also participates in proton transport [26].

To test whether the other V-ATPase subunits phenocopy *VhaPRR*, we used three *GAL4* drivers (*C96*-, *dpp*-, and *ap-GAL4*) to silence a wide panel of V-ATPase subunits. As shown in Table S1, 9 out of 13 subunits tested displayed wing margin defects, which may be caused by defective Wg signaling. Three subunits showed wing hair mispolarization, and two subunits showed notum bristle polarity defects. Knockdown of subunit B (*Vha55*) led to strong PCP defects, but for all other subunits the PCP phenotypes were less severe than those caused by *VhaPRR* knockdown (Figure S7B). The reason for this rather low degree of phenotypic overlap between VhaPRR and other subunits in *Drosophila* phenotypes is unclear. Apart from technical reasons (e.g., ineffective RNAi knockdowns), the redundancy provided by the different Vha subunit paralogs may compensate for the function of other subunits more effectively than the loss of VhaPRR, which is encoded only by one gene and one splice variant. Although further work is needed to characterize the contribution of the individual V-ATPase subunits, our results and those of others suggest that the role of VhaPRR in PCP and Wg signaling is associated with V-ATPase function [18].

Discussion

Our findings identify VhaPRR as a novel regulator of both Wingless and PCP signaling. Our genetic and biochemical analysis proposes a function that is tightly linked to Fz receptors. Very recently, it was described that PRR acts as a specific adaptor between LRP6/arrow and the V-ATPase in the canonical Wnt pathway [18]. This study expands the functional spectrum of VhaPRR and proposes a requirement in the PCP branch of the Wnt pathway where LRP6/arrow does not seem to have a major role [27].

In the pupal wing, we observed impaired Fz localization, irregular cell packing, and defective hair polarization. This complex PCP phenotype of VhaPRR may be caused by the dynamic expression pattern of the V-ATPase in different cellular membranes [4, 28, 29]. In intracellular vesicles, the V-ATPase serves as a pH sensor to regulate trafficking [30]. As such, the V-ATPase might regulate Fz receptor trafficking. A more general role in membrane trafficking might explain additional effects, e.g., on the Notch pathway [28]. However, at least in pupal wings, there seems to be a specific defect in Fz trafficking. Fz is normally transported in vesicles along proximodistally oriented microtubules to distal cell junctions before prehair formation [12]. In *VhaPRR*-silenced cells, Fz accumulates in puncta away from the junctions, suggesting a delay in the vesicular transport of Fz. The observed Fz vesicles do not seem to contain Fmi, which normally travels in the same transport vesicles [12]. Therefore, it will be important to find out whether other properties such as luminal pH and movement behavior are altered in *VhaPRR*-deficient Fz vesicles.

In vesicles and at the plasma membrane, the V-ATPase could also be involved in creating a pH microenvironment that promotes Fz signaling. As shown for other heptahelical transmembrane receptors such as rhodopsin [31], altered proton concentrations could, for example, directly influence Fz signaling by altering Fz conformations within the membrane. Fz is upstream in a signaling cascade that leads to localized actin filament assembly and prehair formation. The restriction of actin-based hair growth to one site in the cell is also dependent on the formin-homology domain containing protein mwh [32, 33]. An interesting link to our data is the recent finding that the formin for3p is regulated by a proton pump in polarized cell growth of fission yeast [34]. Because the organization of the actin cytoskeleton is strongly pH dependent, the V-ATPase may promote actin assembly by regulating local pH [35]. It is therefore intriguing to speculate that pH changes can couple Fz signaling and actin organization to form a part of the cellular machinery that properly localizes wing hair formation.

Proton transporters have been implicated in left-right patterning and tissue regeneration, but the underlying molecular mechanisms remain unclear [36, 37]. Because both processes involve the canonical Wnt and the PCP pathway, our study may provide a basis for mechanistic studies on the role of proton gradients in morphogenetic signaling [38]. Most importantly, the identification of factors that regulate the V-ATPase in this context may also shed light on the missing upstream cues needed for the establishment of planar cell polarity.

Experimental Procedures

Fly Strains and Genetics

Overexpression and transgenic RNAi studies were performed using the UAS/GAL4 system (RNAi crosses grown at 25°C or 29°C; *yw* or an inx2 RNAi were control). *VhaPRR* RNAi lines (5830 or 105281; here termed RNAi-1 and -2, respectively) from the Vienna Drosophila RNAi Center (VDRC) were two nonoverlapping transgenic UAS-RNAi lines, and *VhaPRR[1]* was the *P* element EY03616 from the Bloomington Stock Center (line 15665). *UAS-fz*, *UAS-dsh*, and *UAS-fmi* strains were as described previously [17, 39]. *Ap-GAL4* (Bloomington Stock Center) was a notum and wing disc driver, and *sev-GAL4* (from M. Mlodzik) was an eye-specific driver. *ptc-GAL4* (from N. Perrimon), *dpp-GAL4*, *nub-GAL4*, *C96-GAL4*, and *en-GAL4* (all from the Bloomington Stock Center; the two latter lines also contained UAS-Dicer2) were used for wing expression. To monitor the expression domain of *ptc-GAL4* and *dpp-GAL4*, we coexpressed UAS-GFP. A *wg-lacZ* line (from H. Steller) was used for monitoring *wg* gene expression. *GAL80ts,UAS-Eiger* (from I. Hariharan) was used for apoptotic cell ablation. Excision of the *P* element was mediated by the Δ2-3 transposase generating a revertant chromosome that was viable over the deficiency (*exVhaPRR[1]*). Excision of the *P* element was confirmed by polymerase chain reaction. Transgenic flies expressing PRR-EGFP and *dPRR-mCherry* were provided by M. Boutros [40]. To generate PRRΔC-expressing transgenic flies, we cloned *PRRΔC* (from aa 282–351) into pUAST-attB and injected it into flies with an attP landing site at 86FB by Bestgene.

Histology and Immunohistochemistry

Tangential sections of adult eyes were prepared as described [17]. Wing imaginal discs and pupal wings were dissected, fixed in 4%

paraformaldehyde, and stained according to standard procedure. Extracellular Wingless staining was performed as described [41]. The following primary antibodies were used: mouse anti-Wg (1:50, Developmantal Studies Hybridoma Bank [DSHB]), guinea pig anti-sens (1:1000, by H.J. Bellen), mouse anti-dlp (1:50, DSHB), rabbit anti-Fz2, rat anti-Dll (1:2000 and 1:500, both by S. Cohen), guinea pig anti-arrow (1:200, by S. Eaton), rabbit anti-Fz (1:200, by D. Strutt), rabbit anti-β-gal (1:1000, MP Biomedicals), mouse anti-Fmi (1:50, DSHB), rabbit anti-cleaved Caspase 3 (1:200, Cell Signaling Technology), rabbit anti-engrailed (1:50, Santa Cruz), and rat anti-E-cadherin (1:40, DSHB). Secondary antibodies and rhodamine-phalloidin were obtained from Invitrogen. Images were captured using a Zeiss LSM 510 confocal microscope and were processed with ImageJ and Adobe Photoshop CS4 software. Wings were incubated in isopropanol for 15 min, mounted in Euparal (Roth), and viewed using a Zeiss Axioplan microscope. For electron microscopy, flies were dehydrated in ethanol, isopropanol, and aceton and then dried in a Balzers CPD 020 critical point dryer. Afterward, specimens were coated with gold in a Polaron E500 Cool Sputter Coater and imaged in a Zeiss Leo 430 scanning electron microscope.

Coimmunoprecipitation

Coimmunoprecipitations were performed as described previously [42]. Briefly, HEK293T cells were transiently transfected by the calcium phosphate method with PRR-V5 and FLAG-XFz8, as well as with myc-DFz and myc-DFz2 and the control proteins FLAG-CD2AP and PKD2-V5, respectively. After incubation for 24 hr, cells were washed and lysed in a buffer containing 20 mM Tris-HCl (pH 7.5), 1% Triton X-100, 50 mM NaF, 15 mM Na$_4$P$_2$O$_7$, 0.1 mM EDTA, 150 mM NaCl, 1 mM Na$_3$VO$_4$, and protease inhibitors. After centrifugation (15,000 × g, 30 min, 4°C) and ultracentrifugation (100,000 × g, 30 min, 4°C), cell lysates containing equal amounts of total protein were incubated for 1.5 hr at 4°C with the appropriate antibody, followed by incubation with 25 μl of anti-FLAG M2-beads (Sigma) or V5 antibody-bound protein A Sepharose beads for 3 hr . The beads were washed extensively with lysis buffer, and bound proteins were resolved by SDS-PAGE. Antibodies were rabbit anti-FLAG (1:1000, Sigma), mouse anti-myc 9E10 (1:1000, Santa Cruz), mouse anti-V5 (1:3000, Serotec), and rabbit anti-V5 (1:4000, Sigma).

Supplemental Information

Supplemental Information includes seven figures and one table and can be found with this article online at doi:10.1016/j.cub.2010.05.057.

References

1. Simons, M., and Mlodzik, M. (2008). Planar cell polarity signaling: From fly development to human disease. Annu. Rev. Genet. *42*, 517–540.
2. MacDonald, B.T., Tamai, K., and He, X. (2009). Wnt/beta-catenin signaling: Components, mechanisms, and diseases. Dev. Cell *17*, 9–26.
3. Adler, P.N. (2002). Planar signaling and morphogenesis in Drosophila. Dev. Cell *2*, 525–535.
4. Allan, A.K., Du, J., Davies, S.A., and Dow, J.A. (2005). Genome-wide survey of V-ATPase genes in Drosophila reveals a conserved renal phenotype for lethal alleles. Physiol. Genomics *22*, 128–138.
5. Nguyen, G., Delarue, F., Burcklé, C., Bouzhir, L., Giller, T., and Sraer, J.D. (2002). Pivotal role of the renin/prorenin receptor in angiotensin II production and cellular responses to renin. J. Clin. Invest. *109*, 1417–1427.
6. Nguyen, G., and Muller, D.N. (2010). The biology of the (pro)renin receptor. J. Am. Soc. Nephrol. *21*, 18–23.
7. Simons, M., Gault, W.J., Gotthardt, D., Rohatgi, R., Klein, T.J., Shao, Y., Lee, H.J., Wu, A.L., Fang, Y., Satlin, L.M., et al. (2009). Electrochemical cues regulate assembly of the Frizzled/Dishevelled complex at the plasma membrane during planar epithelial polarization. Nat. Cell Biol. *11*, 286–294.
8. Mummery-Widmer, J.L., Yamazaki, M., Stoeger, T., Novatchkova, M., Bhalerao, S., Chen, D., Dietzl, G., Dickson, B.J., and Knoblich, J.A. (2009). Genome-wide analysis of Notch signalling in Drosophila by transgenic RNAi. Nature *458*, 987–992.
9. Ramser, J., Abidi, F.E., Burckle, C.A., Lenski, C., Toriello, H., Wen, G., Lubs, H.A., Engert, S., Stevenson, R.E., Meindl, A., et al. (2005). A unique exonic splice enhancer mutation in a family with X-linked mental retardation and epilepsy points to a novel role of the renin receptor. Hum. Mol. Genet. *14*, 1019–1027.
10. Wu, J., Klein, T.J., and Mlodzik, M. (2004). Subcellular localization of frizzled receptors, mediated by their cytoplasmic tails, regulates signaling pathway specificity. PLoS Biol. *2*, E158.
11. Krasnow, R.E., and Adler, P.N. (1994). A single frizzled protein has a dual function in tissue polarity. Development *120*, 1883–1893.
12. Shimada, Y., Yonemura, S., Ohkura, H., Strutt, D., and Uemura, T. (2006). Polarized transport of Frizzled along the planar microtubule arrays in Drosophila wing epithelium. Dev. Cell *10*, 209–222.
13. Classen, A.K., Anderson, K.I., Marois, E., and Eaton, S. (2005). Hexagonal packing of Drosophila wing epithelial cells by the planar cell polarity pathway. Dev. Cell *9*, 805–817.
14. Adler, P.N., Liu, J., and Charlton, J. (2000). Cell size and the morphogenesis of wing hairs in Drosophila. Genesis *28*, 82–91.
15. Mlodzik, M. (1999). Planar polarity in the *Drosophila* eye: A multifaceted view of signaling specificity and cross-talk. EMBO J. *18*, 6873–6879.
16. Zheng, L., Zhang, J., and Carthew, R.W. (1995). frizzled regulates mirror-symmetric pattern formation in the Drosophila eye. Development *121*, 3045–3055.
17. Boutros, M., Paricio, N., Strutt, D.I., and Mlodzik, M. (1998). Dishevelled activates JNK and discriminates between JNK pathways in planar polarity and wingless signaling. Cell *94*, 109–118.
18. Cruciat, C.M., Ohkawara, B., Acebron, S.P., Karaulanov, E., Reinhard, C., Ingelfinger, D., Boutros, M., and Niehrs, C. (2010). Requirement of prorenin receptor and vacuolar H+-ATPase-mediated acidification for Wnt signaling. Science *327*, 459–463.
19. Chen, C.M., and Struhl, G. (1999). Wingless transduction by the Frizzled and Frizzled2 proteins of Drosophila. Development *126*, 5441–5452.
20. Rulifson, E.J., and Blair, S.S. (1995). Notch regulates wingless expression and is not required for reception of the paracrine wingless signal during wing margin neurogenesis in Drosophila. Development *121*, 2813–2824.
21. Rulifson, E.J., Micchelli, C.A., Axelrod, J.D., Perrimon, N., and Blair, S.S. (1996). wingless refines its own expression domain on the Drosophila wing margin. Nature *384*, 72–74.
22. Gallet, A., Staccini-Lavenant, L., and Thérond, P.P. (2008). Cellular trafficking of the glypican Dally-like is required for full-strength Hedgehog signaling and wingless transcytosis. Dev. Cell *14*, 712–725.
23. Han, C., Yan, D., Belenkaya, T.Y., and Lin, X. (2005). Drosophila glypicans Dally and Dally-like shape the extracellular Wingless morphogen gradient in the wing disc. Development *132*, 667–679.
24. Cadigan, K.M., Fish, M.P., Rulifson, E.J., and Nusse, R. (1998). Wingless repression of Drosophila frizzled 2 expression shapes the Wingless morphogen gradient in the wing. Cell *93*, 767–777.
25. Piddini, E., Marshall, F., Dubois, L., Hirst, E., and Vincent, J.P. (2005). Arrow (LRP6) and Frizzled2 cooperate to degrade Wingless in Drosophila imaginal discs. Development *132*, 5479–5489.
26. Ludwig, J., Kerscher, S., Brandt, U., Pfeiffer, K., Getlawi, F., Apps, D.K., and Schägger, H. (1998). Identification and characterization of a novel 9.2-kDa membrane sector-associated protein of vacuolar proton-ATPase from chromaffin granules. J. Biol. Chem. *273*, 10939–10947.

27. Wehrli, M., Dougan, S.T., Caldwell, K., O'Keefe, L., Schwartz, S., Vaizel-Ohayon, D., Schejter, E., Tomlinson, A., and DiNardo, S. (2000). arrow encodes an LDL-receptor-related protein essential for Wingless signalling. Nature *407*, 527–530.

28. Yan, Y., Denef, N., and Schüpbach, T. (2009). The vacuolar proton pump, V-ATPase, is required for notch signaling and endosomal trafficking in Drosophila. Dev. Cell *17*, 387–402.

29. Hiesinger, P.R., Fayyazuddin, A., Mehta, S.Q., Rosenmund, T., Schulze, K.L., Zhai, R.G., Verstreken, P., Cao, Y., Zhou, Y., Kunz, J., and Bellen, H.J. (2005). The V-ATPase V0 subunit a1 is required for a late step in synaptic vesicle exocytosis in Drosophila. Cell *121*, 607–620.

30. Hurtado-Lorenzo, A., Skinner, M., El Annan, J., Futai, M., Sun-Wada, G.H., Bourgoin, S., Casanova, J., Wildeman, A., Bechoua, S., Ausiello, D.A., et al. (2006). V-ATPase interacts with ARNO and Arf6 in early endosomes and regulates the protein degradative pathway. Nat. Cell Biol. *8*, 124–136.

31. Mahalingam, M., Martínez-Mayorga, K., Brown, M.F., and Vogel, R. (2008). Two protonation switches control rhodopsin activation in membranes. Proc. Natl. Acad. Sci. USA *105*, 17795–17800.

32. Yan, J., Huen, D., Morely, T., Johnson, G., Gubb, D., Roote, J., and Adler, P.N. (2008). The multiple-wing-hairs gene encodes a novel GBD-FH3 domain-containing protein that functions both prior to and after wing hair initiation. Genetics *180*, 219–228.

33. Strutt, D., and Warrington, S.J. (2008). Planar polarity genes in the Drosophila wing regulate the localisation of the FH3-domain protein Multiple Wing Hairs to control the site of hair production. Development *135*, 3103–3111.

34. Minc, N., and Chang, F. (2010). Electrical control of cell polarization in the fission yeast Schizosaccharomyces pombe. Curr. Biol. *20*, 710–716.

35. Frantz, C., Barreiro, G., Dominguez, L., Chen, X., Eddy, R., Condeelis, J., Kelly, M.J., Jacobson, M.P., and Barber, D.L. (2008). Cofilin is a pH sensor for actin free barbed end formation: Role of phosphoinositide binding. J. Cell Biol. *183*, 865–879.

36. Levin, M., Thorlin, T., Robinson, K.R., Nogi, T., and Mercola, M. (2002). Asymmetries in H+/K+-ATPase and cell membrane potentials comprise a very early step in left-right patterning. Cell *111*, 77–89.

37. Adams, D.S., Robinson, K.R., Fukumoto, T., Yuan, S., Albertson, R.C., Yelick, P., Kuo, L., McSweeney, M., and Levin, M. (2006). Early, H+-V-ATPase-dependent proton flux is necessary for consistent left-right patterning of non-mammalian vertebrates. Development *133*, 1657–1671.

38. Aw, S., and Levin, M. (2009). Is left-right asymmetry a form of planar cell polarity? Development *136*, 355–366.

39. Jenny, A., Darken, R.S., Wilson, P.A., and Mlodzik, M. (2003). Prickle and Strabismus form a functional complex to generate a correct axis during planar cell polarity signaling. EMBO J. *22*, 4409–4420.

40. Buechling, T., Bartscherer, K., Ohkawara, B., Chaudhary, V., Spirohn, K., Niehrs, C., and Boutros, M. (2010). Wnt/Frizzled signaling requires dPRR, the Drosophila homolog of the prorenin receptor. Curr. Biol. *20*, 1263–1268.

41. Strigini, M., and Cohen, S.M. (2000). Wingless gradient formation in the Drosophila wing. Curr. Biol. *10*, 293–300.

42. Simons, M., Gloy, J., Ganner, A., Bullerkotte, A., Bashkurov, M., Krönig, C., Schermer, B., Benzing, T., Cabello, O.A., Jenny, A., et al. (2005). Inversin, the gene product mutated in nephronophthisis type II, functions as a molecular switch between Wnt signaling pathways. Nat. Genet. *37*, 537–543.